Engineering 50 (2025) 96–105

Contents lists available at ScienceDirect

Engineering

journal homepage: www.elsevier.com/locate/eng

Research
Environmental Frontiers for Water–Energy Nexus—Article

Low-Temperature Rapid Drying of Viscous Sludge Via Non-Phase Change Based on Particle High-Speed Self-Rotation and Medium Dispersion in Cyclone

Junjie Liu [a], Qiqi Li [a], Yanan Liang [a], Jianping Li [b], Yi Liu [a], Qiong Li [a], Tingting Cheng [a], Aosong Wei [a], Shenggui Ma [b], Xia Jiang [b], Hualin Wang [a], Pengbo Fu [a,*]

[a] National Engineering Research Center of Industrial Wastewater Detoxication and Resource Recovery, East China University of Science and Technology, Shanghai 200237, China
[b] National Engineering Research Center for Flue Gas Desulfurization, Sichuan University, Chengdu 610065, China

ARTICLE INFO

Article history:
Received 25 November 2023
Revised 25 September 2024
Accepted 24 October 2024
Available online 6 November 2024

Keywords:
Sludge drying
Cyclone
Particle high-speed self-rotation
Viscous sludge
Dispersed phase medium (DPM)
Non-phase change

ABSTRACT

Drying operations are of grave importance to realize the reduction and utilization of sewage sludge resources, but the conventional thermal evaporation drying (TED) technology presents challenges due to the need for a large amount of thermal energy to conquer the phase-change latent heat of moisture. Herein, we report a non-phase change technology based on particle high-speed self-rotation in a cyclone for fast, low-temperature drying of viscous sludge with high-moisture contents. Dispersed phase medium (DPM) is introduced into the cyclone self-rotation drying (CSRD) reactor to enhance the dispersion of the viscous sludge. The effects of carrier gas temperature, feeding rate, size, and proportion of DPM particles in the drying process are systematically examined. Under optimal operating conditions, the weighted content of moisture in the viscous sludge could be reduced from 80% to 15.01% in less than 5 s, achieving a high drying efficiency of 95.79%. Theoretical calculations also reveal that 89.26% of the moisture is removed through non-phase change pathway, contributing to a 522-fold increase in the drying rate of CSRD compared to TED technology. This investigation presents a sustainable effective approach for high moisture viscous sludge treatment with low energy consumption and carbon emissions.

© 2024 THE AUTHORS. Published by Elsevier LTD on behalf of Chinese Academy of Engineering and Higher Education Press Limited Company. This is an open access article under the CC BY-NC-ND license (http://creativecommons.org/licenses/by-nc-nd/4.0/).

1. Introduction

The rapid development of cities and industries leads to the mass production of sewage sludge as a byproduct of the sewage treatment process with characteristics such as high humidity, large volume, toxicity, and strong odor [1–5]. In the past decade, the average sludge produced annually in the United States was 17.8 million tonnes of dry matter [6]. In 2020, China's wet sludge production (moisture: 80%) exceeded 72 million tonnes and is expected to exceed 90 million tonnes in 2025 [7]. The reduction, stabilization, harmlessness, and exploitation of sludge resources are of great significance for sustainable development.

Due to the toxicity of sludge and the scarcity of land resources [8–10], the proportion of landfilling has remarkably reduced, and also direct landfilling has been prohibited in many areas [11–13]. The efficient use of resources has become the focus of development for the treatment and disposal of sludge [14–17]. For the as-developed resource approaches, such as incineration, pyrolysis, and building materials utilization, the benefits highly depend on the efficiency of moisture removal from the sludge [7,18,19]. Sludge drying is able to substantially decrease its volume and mass; for example, by lowering the moisture content from 80% to 30%, the mass can be reduced by 28.6%. Normally, the sludge moisture can be reduced by pre-dewatering and drying operations [20,21]. Unfortunately, most industrial sludge collected from pre-dewatering devices is viscous sludge containing over 80% [22–24], and drying this type of high-moisture content viscous sludge remains a significant industrial challenge.

The conventional drying methods, such as belt drying, rotary drying, paddle drying, and thin layer drying [25–27], are mainly designed based on the principle of phase change evaporation, where heat conduction for water to vapor phase conversion is uti-

* Corresponding author.
E-mail address: fupb@ecust.edu.cn (P. Fu).

https://doi.org/10.1016/j.eng.2024.10.012
2095-8099/© 2024 THE AUTHORS. Published by Elsevier LTD on behalf of Chinese Academy of Engineering and Higher Education Press Limited Company.
This is an open access article under the CC BY-NC-ND license (http://creativecommons.org/licenses/by-nc-nd/4.0/).

lized, thereby achieving liquid and dry matter separation [28,29]. However, thermal evaporation drying (TED) is theoretically considered an energy-intensive process because the latent heat for vaporization of water is as high as 2258 $kJ \cdot kg^{-1}$ [30]. For instance, in the United States, the energy consumed in the separation process makes up 45% to 55% of industrial energy consumption; specifically, the energy used for thermal separation, such as evaporation, accounts for 80% of the entire separation process [31]. Additionally, it usually takes a long time for the water to completely evaporate from the viscous sludge. As a result, a fast and efficient approach for the treatment of dispersed viscous sludge with low energy consumption is urgently desired.

As a typical non-thermal separation equipment, the cyclone has been extensively employed in the field of material separation. Utilizing advanced theoretical and characterization calculations, our team has discovered that particles in a cyclone exhibit a dual rotation phenomenon. Not only do they rotate around the axis of the cyclone, but they also undergo a rapid self-rotation around their center at a remarkable speed of 2000–6000 $rad \cdot s^{-1}$ [32,33]. Taking advantage of this feature, a series of novel cyclone technologies were developed for industrial applications, such as oil–water separation [34–37], self-rotation-enhanced wastewater anoxic/aerobic process [38], catalyst self-rotation activation [39], and cyclonic absorption [40]. We have also demonstrated a principle for non-phase change drying based on the particle high-speed self-rotation in cyclones. Under low carrier gas temperatures (< 100 °C), sludge and lignite were also dried with a moisture content of 53% [41] and 45% [42] in short residence time (< 15 s), with a high drying efficiency of greater than 90%. This cyclone self-rotation drying (CSRD) process has obvious advantages in terms of energy consumption compared to conventional TED technologies; nevertheless, our previous research [41,42] essentially concentrated on solidified sludges with moisture content below 60%. For viscous sludges with a moisture content greater than 70% or even above 80%, the effectiveness of CSRD is limited due to poor dispersion of the sludge in the cyclone and particle adhesion to the cyclone wall.

To solve the above bottlenecks, this study aims to establish a novel non-phase change strategy for rapid drying of high-moisture viscous sludge at low temperatures. By taking advantage of the high-speed self-rotation of the sludge particles in the cyclone and the dispersing effect of the dispersed phase medium (DPM) on the sludge, we eliminate the need for moisture in raw sludge for non-phase change CSRD, thereby reducing the energy consumption for sludge drying. Our further investigations reveal that under the temperature of 70 °C, a striking drying efficiency of more than 95% could be achieved in less than 5 s, and the DPM is recycled for further use. This study is effectively aimed to suggest a novel pathway to treat sludge with low energy consumption, benefiting low carbon development.

2. Materials and methods

2.1. Experimental principles

Sludge with 80% moisture content will be in a highly aggregated state and cannot be uniformly dispersed in a cyclone; therefore, it cannot be directly dried by cyclone self-rotation. To improve the dispersibility of viscous sludge, a DPM was introduced to form a sludge–sand mixture through the adhesion of quartz sand particles. Fig. 1 demonstrates the principle of self-rotation drying of viscous sludge in a cyclone dryer. After the sludge–sand mixture is transferred from the tangential inlet to the cyclone dryer by the

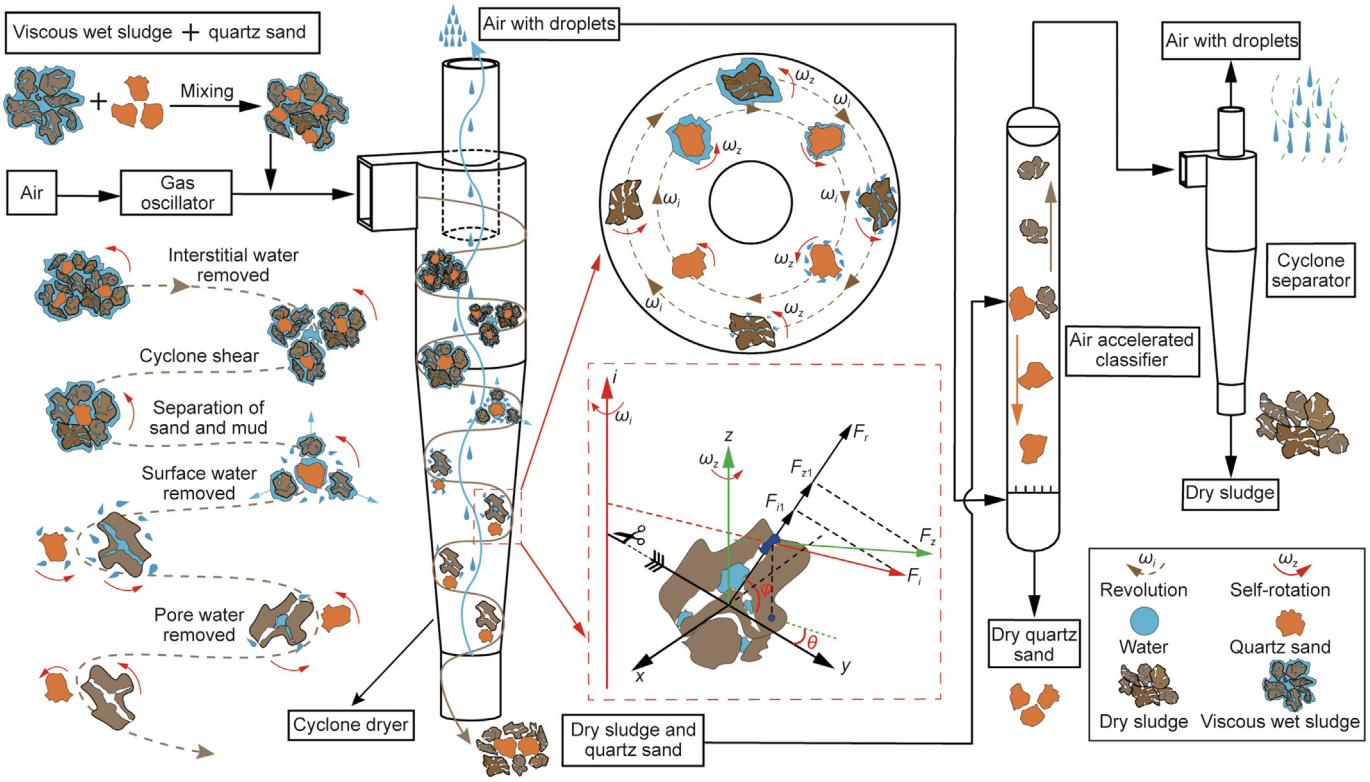

Fig. 1. Principle for the low-temperature non-phase change drying of viscous sludge based on particle high-speed self-rotation and medium dispersion in a cyclone. The definitions of the variables could be found in Section 2.1.

carrier gas, the mixture changes from a linear motion to a helical motion under the effect of the tangential flow, which appears as a rotational motion around the central axis of the cyclone. Since the density of the sludge–sand mixture is higher than that of the carrier gas, the sludge–sand mixture radially migrates to the vicinity of the cyclone dryer walls under the influence of centrifugal force, thereby separating the sludge and sand from the carrier gas. Under the action of the flow field of the cyclone dryer, the quartz sand particles attached to the wet sludge exhibit high-speed rotation with a speed in the range of 2000–6000 rad·s^{-1} [32,33]. Under the coupled centrifugal force of the self-rotation and rotational motion of particles, the moisture presents in various states, such as free water, interstitial water, and surface water, and migrates into the gas phase in the form of micro-droplets [43]. The direction of the high-speed self-rotation of the particles in the cyclone dryer is opposite to the direction of revolution. As a result, the moisture in the sludge can be effectively removed under the action of the coupled centrifugal force generated by high-speed self-rotation and rotational motions.

The coupled centrifugal separation factor (F_r) can be calculated as follows [42,44]:

$$F_r = F_{z1} + F_{i1} = \frac{r\omega_z^2}{g}\cos^2\varphi + \frac{(r\cos\varphi\cos\theta + R)\omega_i^2}{g}\cos\varphi \quad (1)$$

where F_z and F_i represent the centrifugal forces of self-rotation and revolution, respectively; F_{z1} and F_{i1} represent the centrifugal separation factors of self-rotation and revolution in the radial direction, respectively; r signifies the distance from the center of the liquid droplet to the center of the sludge particle; ω_z and ω_i represent the speed of particle self-rotation and revolution in the cyclone, respectively; g is the acceleration of gravity; R denotes the distance from the center of the particle to the central axis of the cyclone; φ is the azimuth angle (the angle between the line connecting the channel droplet and the center of the sludge particle and the *xoy* plane); and θ is the polar angle (the angle between the projection of the line connecting the droplet and the center of the sludge particle on the *xoy* plane and the *y*-axis).

In this study, dry sludge particles and quartz sand particles fall from the bottom outlet of the cyclone dryer into the middle of the air-accelerated classifier (AAC). The airflow carries the micro-droplets out of the overflow port of the cyclone separator (CS) and then enters the lower part of the AAC. Under the sorting action of the pulsating airflow, the quartz sand particles are discharged from the bottom of the AAC to the recirculation system, while the air carries the dry sludge from the top of the AAC into the CS.

2.2. Materials

The material used in this study was landfill sludge obtained from the Shanghai Laogang sludge landfill site. The moisture content of the sludge was approximately 80%, and more information on the test materials can be found in Text S1 and Table S1 in Appendix A. The conducted thermogravimetric analysis revealed that the content of organic matter in the raw sludge was remarkably low (Fig. S1 and Text S2 in Appendix A), which could be attributed to the presence of anaerobic fermentation of the sludge for several years.

2.3. Experimental device and process

Figs. 2(a)–(d) illustrate the CSRD process of the viscous sludge, a three-dimensional diagram, and an on-site image of the device, respectively. The testing process can be divided into three parts. The first is the carrier gas system, where the air passes through the fan and electric heater to form a hot carrier gas. The second is the feeding system, in which wet sludge and quartz sand are mixed in a mixer at a certain ratio, and then transported by a screw feeder. The third system is the drying and classification system.

In this system, the hot carrier gas takes the sludge and sand mixture to the cyclone dryer. The quartz sand particles are discharged from the bottom of the AAC through airflow separation. The dried sludge enters the CS from the top of the AAC along with the airflow, thus realizing the separation of the dry sludge and the carrier gas containing fine droplets. The nominal diameter of the cyclone dryer and CS (Fig. 2(e)) are both 200 mm, but the difference in structure is mainly due to different functions. The principle of separation of DPM and dry sludge in AAC is given in some detail in Text S3 and Fig. S2 in Appendix A.

2.4. Analysis and calculation methods

Text S4 in Appendix A presents the methods used for determining the moisture content of sludge, the calculation of the drying efficiency, together with the instrument information for sample characterizations.

3. Results and discussion

3.1. Impacts of the quartz sand particle size on the CSRD of sludge

The effects of various particle sizes of the quartz sand on the CSRD of the sludge were methodically examined under the conditions of maintaining the system air volume at 650 m^3·h^{-1}, carrier gas temperature at 70 °C, feeding rate of 30 kg·h^{-1}, and sand–sludge mixing ratio 3:1. In the actual experiment, the quartz sand particles cannot be completely separated from the sludge attached to the surface. Hence, a certain amount of unseparated sludge is carried by the discharged quartz sand. The purities of the sludge and quartz sand at each outlet in the drying process were also systematically analyzed.

The plotted results in Fig. 3(a) reveal that the larger the quartz sand particles, the worse the sludge drying effect. This is essentially related to the fact that the larger the particle size, the lower the self-rotation speed in the cyclone. When the particle size was greater than 4 mm, the drying efficiency of sludge carried by quartz sand was obtained as only 24.47% (absolute sludge water content decreased from 4.00 to 3.02 g·g^{-1} dry sludge). The residual moisture content of the sludge carried by the quartz sand and the final product sludge was weighted according to the mass ratio; which could represent the overall drying effect of the sludge (Text S4 in Appendix A for analysis and calculation methods). As illustrated in Fig. 3(b), the overall weighted drying efficiency curve of the total sludge exhibits a downward trend with increasing quartz sand particle size, which indicates that decreasing the particle size can be beneficial for sludge drying. When the particle size was less than 3 mm, the weighted drying efficiency was higher than 79.68%.

Fig. 3(c) demonstrates that with increasing particle size, the amount of sludge carried by quartz sand at the outlet from the bottom of AAC increases, while the amount of quartz sand in the dried sludge at the outlet of CS decreases. This is essentially caused by the much lower self-rotation speed of large-grained quartz sand with attached sludge. As illustrated in Fig. 3(d), when the particle size was in the range of 0–1 mm, the quartz sand and dried sludge were completely removed from the CS. This means that separation between the dried sludge and DPM is not achieved. In addition, the DPM reuse is not achievable, and sludge purity may also be affected. To achieve the highest efficiency of sludge drying and sludge and sand separation, the optimal particle size was set in the range of 2–3 mm. Text S5 and Fig. S3 in Appendix A show the state and particle size of the inlet and outlet sludge during the experiment. The obtained results revealed that the average

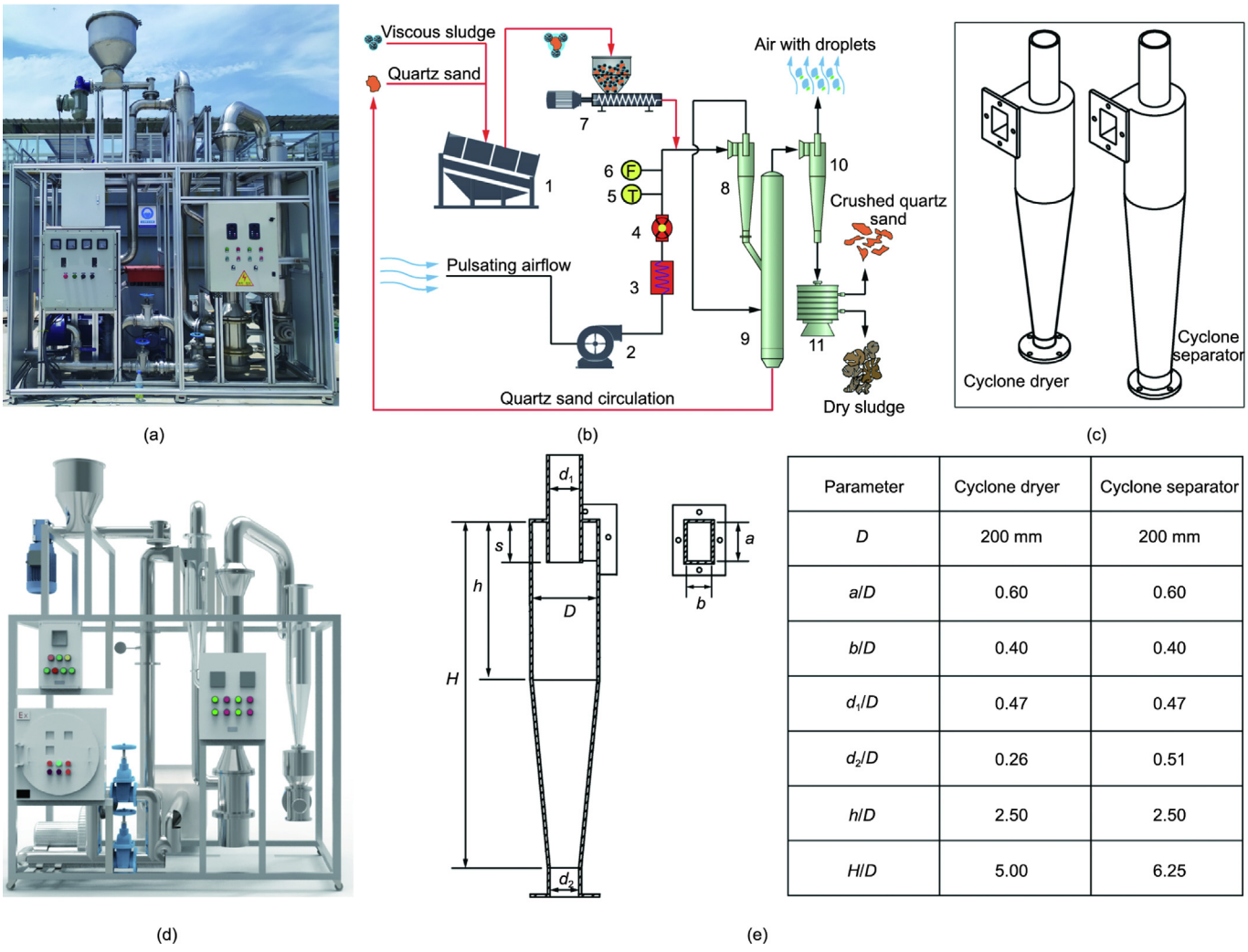

Parameter	Cyclone dryer	Cyclone separator
D	200 mm	200 mm
a/D	0.60	0.60
b/D	0.40	0.40
d_1/D	0.47	0.47
d_2/D	0.26	0.51
h/D	2.50	2.50
H/D	5.00	6.25

Fig. 2. Process flow and device: (a) physical image of the device; (b) process flow; (c) three-dimensional diagram of the cyclone dryer and separator; (d) three-dimensional diagram of the device; and (e) size of the cyclone dryer and separator, 1: mixer; 2: fan; 3: electric heater; 4: gas oscillator; 5: thermometer; 6: flow meter; 7: screw feeder; 8: cyclone dryer; 9: air accelerated classifier; 10: cyclone separator; 11: classifying sieve. s, h, H, D, d_1, d_2, a, and b are the parameters of the cyclone dryer and separator.

particle size of the raw sludge was 34.05 μm, while the average particle size of the dried sludge output from CS was 796.50 μm. This difference can be attributed to the fact that the initial state of the raw sludge was viscous and semi-solid, while the addition of solvent improved the dispersion during the particle size test and formed isolated sludge particles of small sizes. In the drying process, the removal of moisture causes these sludge particles to solidify and produce large aggregates with a stable particle shape.

3.2. Impacts of the sludge–sand mixing ratio on the CSRD of sludge

The CSRD of viscous sludge is based on the mixing of sludge and quartz sand to improve the dispersibility of the sludge and increase the gas–liquid contact area. Hence, the mixing ratio of the sludge and sand is a crucial influencing factor. Fig. 4(a) illustrates that with the increase of sand–sludge mixing ratio, the efficiency of sludge drying exhibits a tendency to increase at first and then decrease. By increasing the mixing ratio, the overall dispersion degree of the viscous sludge is improved and thus the drying efficiency is improved. When the mixing ratio is further increased, the carrier gas load is excessive; as a result, the drying efficiency is reduced.

Fig. 4(b) demonstrates that the weighted drying efficiency of sludge first increases and then decreases with increasing mixing ratio. When the mixing ratio was 3.5:1.0, the maximum drying efficiency was 89.94% and the moisture content by weight was 28.58%. As illustrated in Fig. 4(c), the purity of quartz sand discharged from the bottom of AAC is positively correlated with the mixing ratio, and the purity of sludge at the bottom outlet of CS is generally negatively correlated with the mixing ratio. As the mixing ratio increases, the ratio of the sludge discharged from the CS bottom to the total feeding sludge also increases. As demonstrated in Fig. 4(d), when the mixing ratio increases from 2.0:1.0 to 4.0:1.0, this ratio rises from 38% to 70%. This is mainly because a higher mixing ratio increases the degree of separation between the sludge and sand. By comprehensively considering the drying effect and classification efficiency, the optimal mixing ratio was determined to be 3.0:1.0. It should be noted that the experimental results are substantially influenced by the sludge viscosity. When sludge with higher initial moisture (85%; lower viscosity) was utilized for comparative experiments, the law obtained was almost identical (Text S6 and Fig. S4 in Appendix A).

3.3. Impacts of the carrier gas temperature on the sludge CSRD

Increasing carrier gas temperature is able to reduce the viscous resistance of moisture both on the surface and in the pores of sludge particles [45]. Therefore, a higher gas temperature is

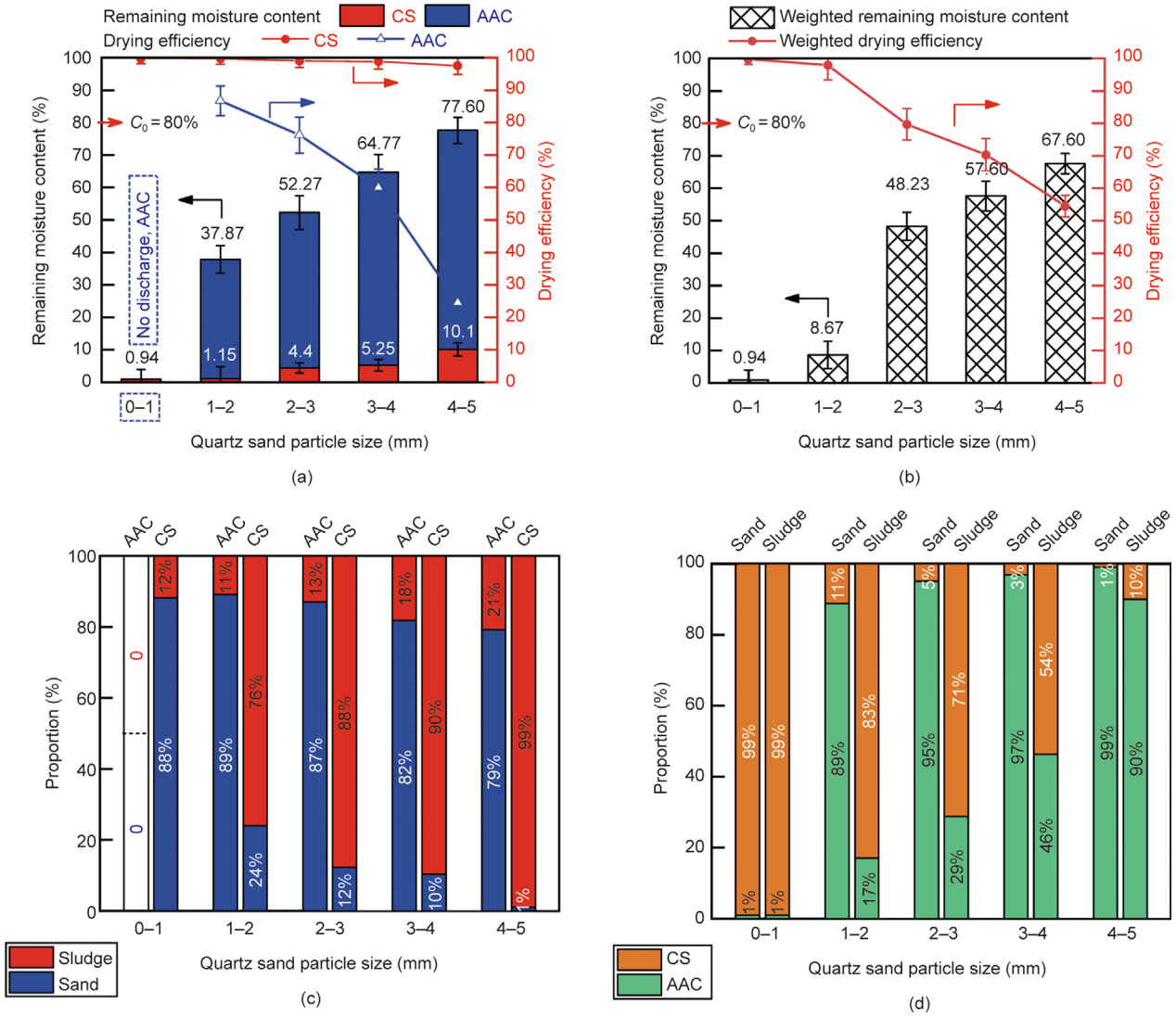

Fig. 3. Effects of the size of quartz sand particles on the CSRD (conditions: at a carrier gas temperature of 70 °C, feeding rate of 30 kg·h^{-1}, and sand–sludge ratio of 3:1): (a) drying efficiency, C_0 represents initial moisture content of raw material; (b) weighted drying efficiency; (c) proportions of sludge and sand at the outlet; and (d) proportion of material flow.

favorable for moisture removal by cyclone self-rotation. Fig. 5(a) demonstrates the effect of temperature on the sludge CSRD. Under normal temperature conditions (30 °C), the moisture content of raw sludge can be reduced from 80% to 10.30% after drying (drying efficiency 97.09%), and the moisture content of the sludge carried by the quartz sand could be reduced to 58.22% (drying efficiency of 65.16%). The weighted moisture content of the sludge after the CSRD was 50.08%, and the weighted drying efficiency could reach 69.60%.

In this system, the sludge residence time in the cyclone dryer was less than 5 s. There was no time for the moisture in the sludge to vaporize and evaporate in a few seconds at low temperatures, indicating that the CSRD process is not primarily based on phase change. After increasing the temperature of the carrier gas, due to the decrease in moisture viscosity, the weighted moisture content of the sludge continued to decrease, but the decrease in moisture gradually decelerated. Fig. 5(b) illustrates that with the increase in carrier gas temperature, the weighted drying efficiency of sludge enhances from 50.08% to 94.61%, and the upward trend of drying efficiency is more evident in the temperature range of 50 to 70 °C. This may be related to the increase in the sludge–moisture interaction force with decreasing moisture content. Therefore, to achieve a balance between energy and efficiency, the temperature should be controlled around 70 °C.

The ratios of discharged sludge and sand were also appropriately analyzed. As illustrated in Fig. 5(c), the purity of quartz sand in the bottom outlet of AAC is relatively high, with values between 87% and 94%. Fig. 5(d) illustrates that 89%–98% of the quartz sand is discharged from the bottom of the AAC. In terms of sludge distribution, the proportion of sludge discharged from the CS bottom to total sludge increased with the growth of carrier gas temperature. As the carrier gas temperature increases, both the degree of sludge drying and the degree of separation of sludge and sand exhibit an ascending trend. Additionally, the conclusion about carrier gas temperature can be well confirmed by control experiments (Text S7 in Appendix A), in which the feeding rate or mixing ratio of sludge to sand was varied while keeping other conditions constant (Fig. S5 and Fig. S6 in Appendix A).

The characteristics of sludge pore distribution before and after drying were measured by nitrogen adsorption and mercury intrusion methods. According to Table 1 and Text S8 in Appendix A, cyclone drying increased the porosity and pore volume of the raw sludge, together with a distinct increase in the average pore diameter from 94.38 to 413.02 nm. Analysis of pore size

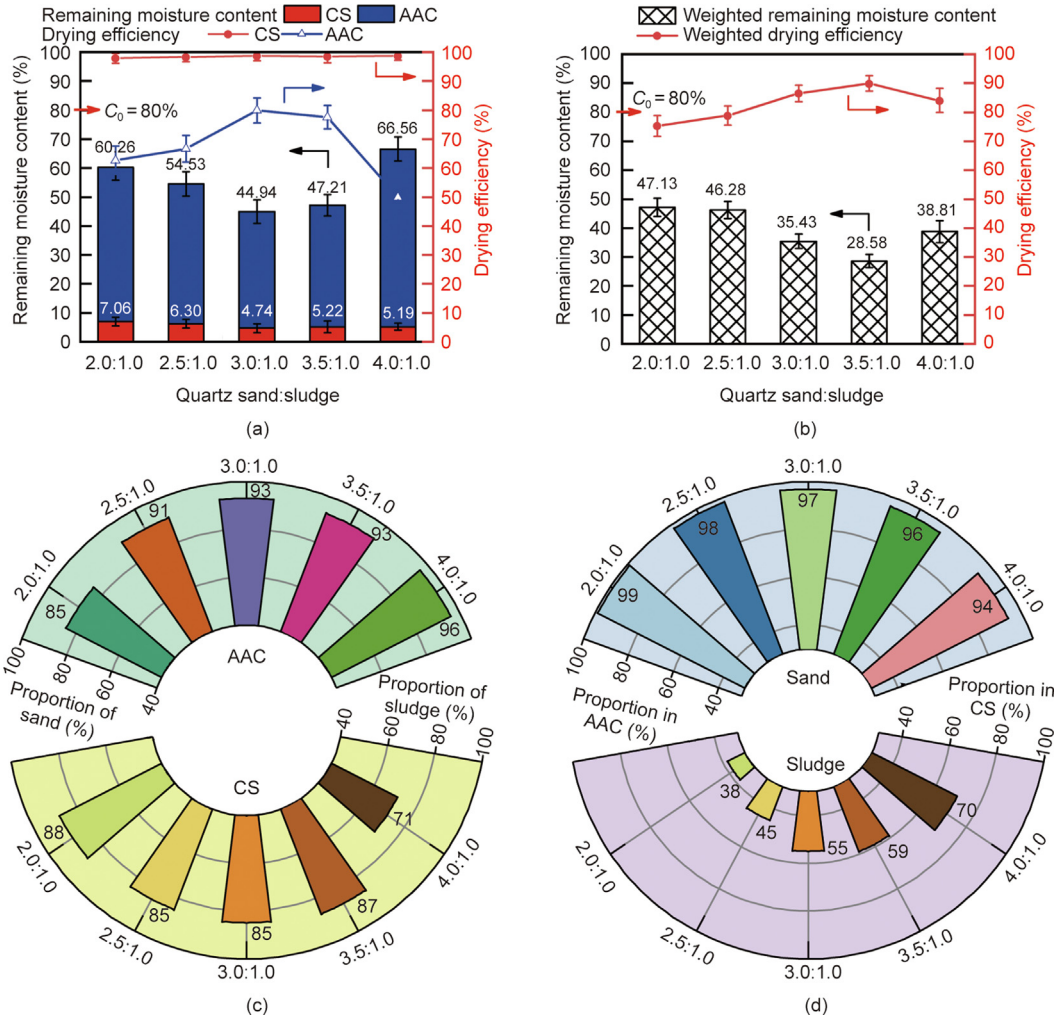

Fig. 4. Effects of the mixing ratio on the CSRD (conditions: raw sludge moisture content of 80%, carrier gas temperature of 70 °C, feeding rate of 60 kg·h^{-1}, and quartz sand particle size range of 2–3 mm): (a) drying efficiency; (b) weighted drying efficiency; (c) proportions of sludge and sand at the outlet; and (d) proportion of material flow.

distribution (Fig. S7 in Appendix A) further revealed the increased amounts of large pores with sizes greater than 3 μm. Based on the above discussion, this is caused by the agglomeration of wet sludge into large particles during cyclone drying under the influence of the carrier gas temperature, which increases the number of stacked interstitial pores.

After CSRD, the bulk density of sludge slightly lessened, which was directly related to the increase of sludge pore volume and median particle size (Text S5 and Fig. S3). Before and after self-rotation drying, the pore area of the sludge decreased from 15.808 to 4.897 m^2·g^{-1}, because the number of pores with a diameter less than 3 μm decreased. Nitrogen adsorption measurements showed that cyclone drying reduced the pore volume from 0.0556 to 0.0137 cm^3·g^{-1}, but little changed the average pore diameter of the sludge. This indicates a substantial reduction in the number of mesopores due to drying. Fig. S7(b) illustrates the mercury adsorption and desorption curves of the samples before and after sludge drying. The sludge dried under the same pressure exhibited a higher degree of mercury inhalation. Moreover, the desorption and adsorption curves displayed a better fit compared to the raw sludge. This indicates that the connectivity between pores in dried sludge particles is better, which is also related to the increase in the number of macropores.

Text S9 and Fig. S8 in Appendix A illustrate scanning electron microscope (SEM) images of sludge samples before and after drying. From Figs. S8(c) and (d), a state of particle aggregation can be clearly observed on the raw sludge surface, where there are evident cracks between the sludge particles as well as numerous mesoporous structures on the sludge particle surface. These structures absorb a large amount of moisture, which will be more difficult to remove due to capillary forces. The surface of the dried sludge particles is smoother and the number of mesopores is remarkably reduced (Figs. S8(g) and (h)). This may be because the sludge particles are squeezed by the CS sidewalls and sheared by the cyclone during the CSRD process, which is consistent with the results of the nitrogen adsorption method.

3.4. Impacts of the feeding rate on the sludge CSRD

The feeding rate can change the particle collision probability and affect the heat transfer process between the carrier gas and the material, thereby affecting the particle's self-rotation speed and moisture removal efficiency. As can be seen from Figs. 6(a) and (b), the moisture content of sludge carried by the quartz sand and that of the sludge discharged from CS grows with increasing the feeding rate. However, the drying efficiency plot exhibits a decreasing trend, inducing a peak efficiency at a feeding rate of 30 kg·h^{-1}. This may be because this feeding rate could ensure sufficient self-rotation movement of the particles and maximize the collision probability between them, thereby enhancing the overall

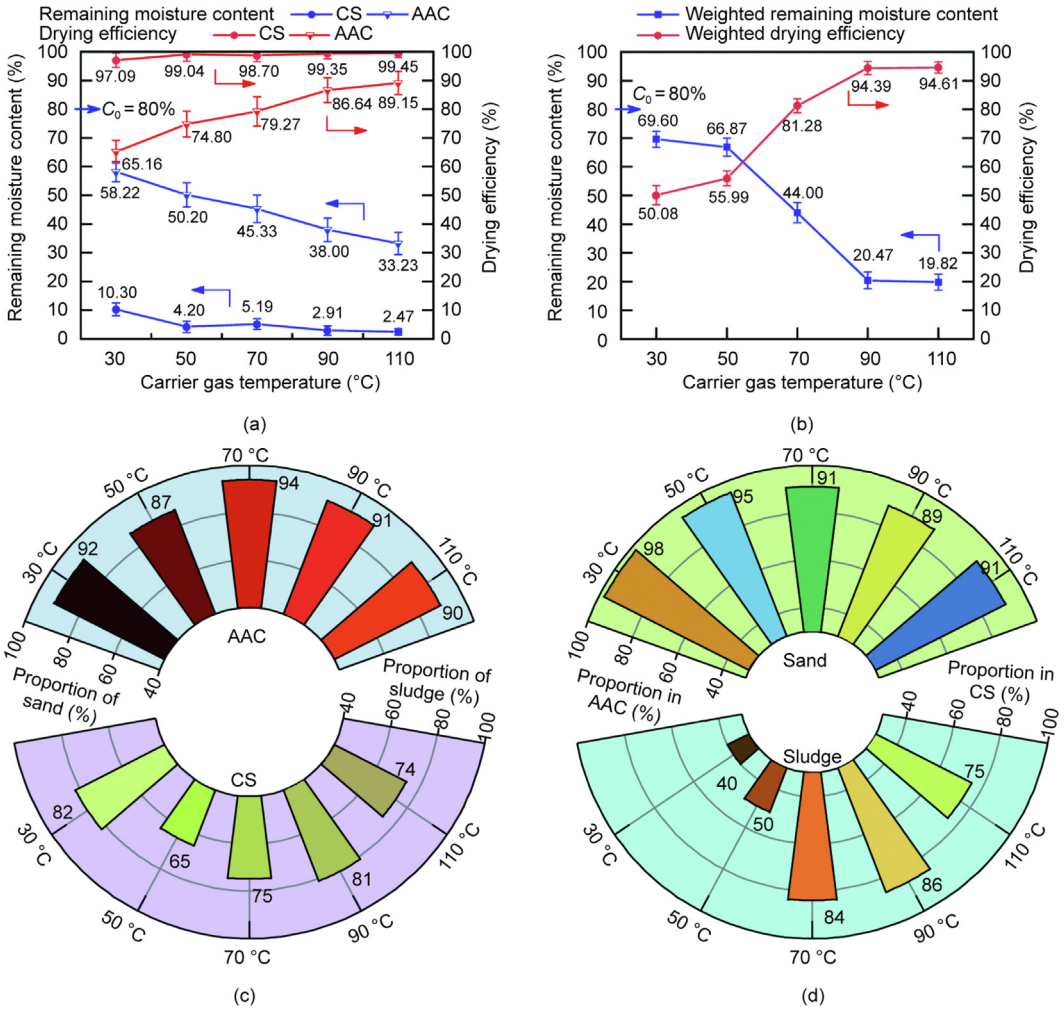

Fig. 5. Effects of the carrier gas temperature on the CSRD (conditions: feeding rate of 30 kg·h^{-1}, sand–sludge mixing ratio of 3:1, and sand particle size range of 2–3 mm): (a) drying efficiency; (b) weighted drying efficiency; (c) proportions of sludge and sand at the outlet; and (d) proportion of material flow.

Table 1
Pore characteristics of sludge before and after drying.

Sample	Mercury intrusion (> 50 nm)					Nitrogen adsorption (< 50 nm)	
	Porosity (%)	Pore volume (mL·g^{-1})	Average pore size (nm)	Pore area (m^2·g^{-1})	Bulk density (g·mL^{-1})	Average pore size (nm)	Pore volume (cm^3·g^{-1})
Original sludge	44.78	0.3730	94.38	15.808	1.2006	26.582	0.0556
Dried sludge	51.43	0.5056	413.02	4.897	1.0171	29.992	0.0137

drying efficiency. At this time, the weighted content of residual moisture of the sludge could be reduced from 80% to 15.01%, and a drying efficiency of 95.79% can be obtained.

As presented in Figs. 6(c) and (d), the ratio of quartz sand at the AAC bottom to the total quartz sand gradually increases with the growth of the feeding rate, and the ratio of the sludge discharged from the CS to the total sludge gradually decreases. Considering several critical factors such as drying efficiency, purity of discharged sludge, and flow direction of sludge products, the optimal feeding rate should be set to 30 kg·h^{-1}. The impact of the feeding rate on the CSRD at high carrier gas temperatures was investigated by setting the carrier gas temperature at 90℃. The obtained results in Text S10 and Fig. S9 in Appendix A display that the optimal feeding rate is still 30 kg·h^{-1}. The effects of airflow pulsation frequency on the CSRD are detailed in Text S11 and Fig. S10 in Appendix A. The attained results indicate that the weighted drying efficiency of sludge rises with increasing the pulsation frequency.

3.5. Proportion of non-phase change in the CSRD process

To compare the drying rates of the TED and CSRD, another set of constant-temperature drying experiments was conducted at 70 °C. The change in the moisture content of the sludge during the drying experiments was recorded in real-time, and the corresponding results have been presented in Text S12 and Fig. S11 in Appendix A. After the CSRD process, the moisture content of the sludge decreased from 84.76% to 4.81% within 5 s, while it took approximately 95 min for the TED technology. As time went by, the TED drying rate exhibited rapid growth at first, followed by a gradual lessening, with a maximum drying rate of 0.0025 g·s^{-1}. In comparison, the average drying rate of the CSRD was as high as 1.38 g·s^{-1},

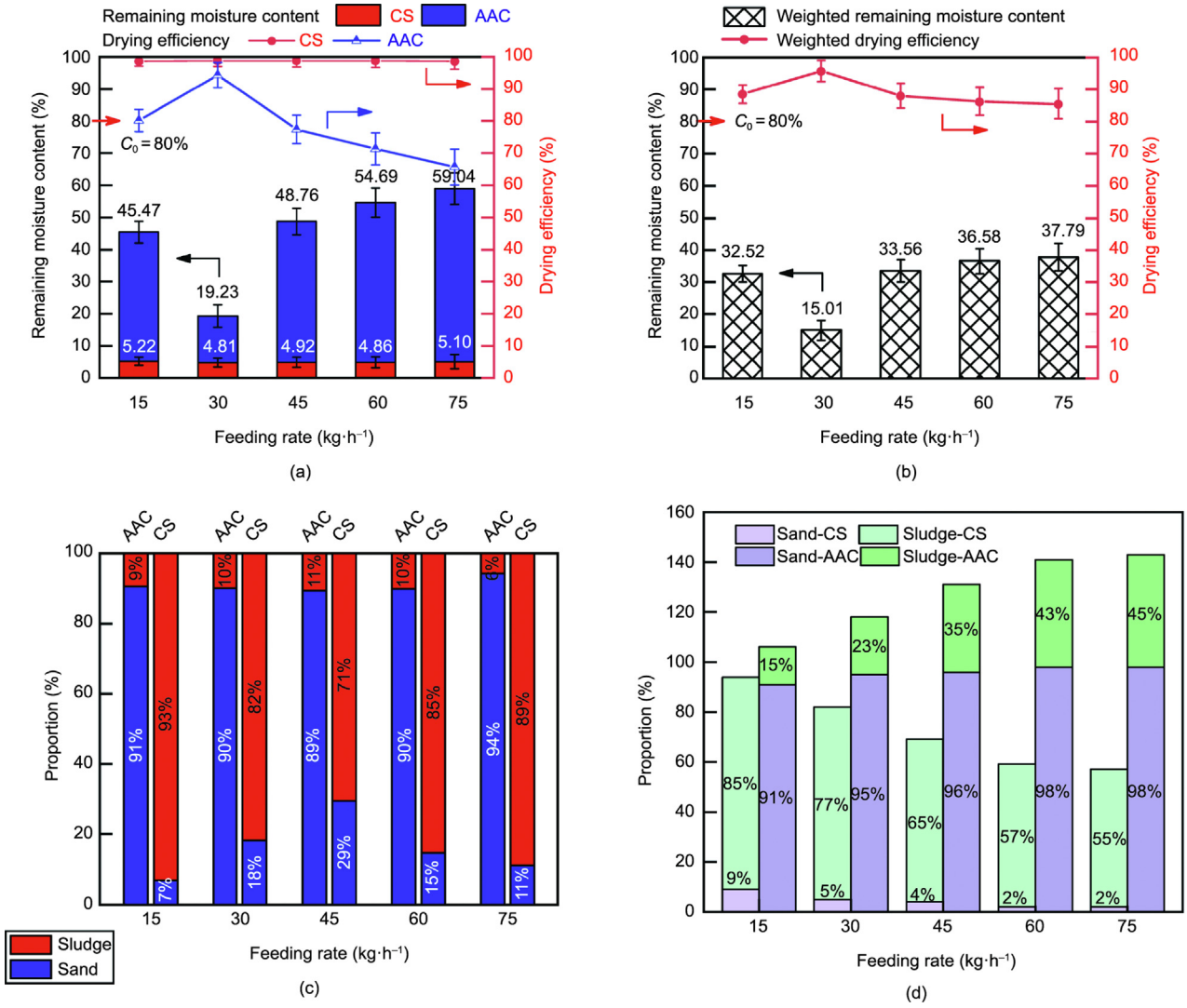

Fig. 6. Effects of the feeding rate on the CSRD (conditions: carrier gas temperature of 70 °C, sand–sludge mixing ratio of 3:1, and sand particle size range of 2–3 mm): (a) drying efficiency; (b) weighted drying efficiency; (c) proportions of sludge and sand at the outlet; and (d) proportion of material flow.

which was 552 times higher than that of the TED. In summary, the CSRD sludge requires significantly less drying time at the same temperature and exhibits higher drying efficiency.

Theoretical calculations were performed to estimate the non-phase change ratio during sludge drying. It is assumed that all molecules evaporated from the liquid surface during the drying process do not recondense due to collisions with other molecules. As explained in Text S13 and Table S2 in Appendix A, u (liquid evaporation rate) is the rate of lowering of the liquid surface, which is equal to the molecular flux of evaporation divided by the molecular number density of the liquid, as well as the molecular flux of condensation divided by the molecular number density of the liquid. For saturated steam as an ideal gas, J represents the number of molecules condensed on the surface of a unit liquid per unit time; P denotes the pressure of the saturated steam; T is the thermodynamic temperature; v is the average velocity of the molecules; n_g denotes the molecular number density; ρ_g is the gas density; m is the mass of the molecule; M is the molar mass; n_1 is the molecular number density of the liquid, and ρ_1 is the liquid density; and R is the universal gas constant. The calculation process for the drop rate of the liquid level u is provided in the following:

$$u = \frac{J}{n_1} = \frac{n_g v}{4n_1} = \frac{m n_g v}{4 m n_1} = \frac{\rho_g v}{4\rho_1} = \frac{\frac{MP}{RT} \times \sqrt{\frac{8RT}{\pi M}}}{4\rho_1} = \left(\frac{P}{\rho_1}\right)\sqrt{\frac{M}{2\pi RT}} \quad (2)$$

The total volume of the added quartz sand (V_1) and the volume of a single quartz sand particle (V_2) was calculated from the relationship between the mass and density (ρ) of the quartz sand being added. Herein, the quartz sand particles were approximated as spheres, and thereby, their relations are as follows:

$$V_1 = \frac{M}{\rho} \quad (3)$$

$$V_2 = \frac{4}{3}\pi\left(\frac{r}{2}\right)^3 \quad (4)$$

The number of quartz sand particles (N) can be also obtained by:

$$N = \frac{V_1}{V_2} \quad (5)$$

The surface area (S_0) of a single quartz sand particle and the total surface area (S_1) of the added quartz sand particles could be deduced.

$$S_0 = 4\pi\left(\frac{R}{2}\right)^2 \tag{6}$$

$$S_1 = N \times S_0 \tag{7}$$

The liquid evaporation rate (V) can be then calculated based on the following relation:

$$V = S_1 \times u \tag{8}$$

The residence time of the sludge material in the CSRD system from feed to discharge is T_0, the liquid evaporation (Q) could then be obtained as:

$$Q = V \times T_0 \tag{9}$$

The mass of dried sludge (m_1) could be calculated, where w_1 is the initial moisture content of the sludge, w_2 is the remaining moisture content (weighted), and E is the drying efficiency (weighted), which leads to the total moisture removal amount from the wet sludge (m_2) as follows:

$$m_1 = \frac{mw_1(1-E)}{w_2} \tag{10}$$

$$m_2 = mw_1 - m_1w_2 \tag{11}$$

The proportion of the non-phase change removal of the moisture (ω) can be calculated by:

$$\omega = \frac{m_2 - Q}{m_2} \times 100\% \tag{12}$$

After plugging the data from Table S2 in Appendix A into the equations above, we found that 89.26% of the moisture removed in the CSRD process is due to non-phase change. This indicates that the CSRD process removes moisture differently compared to conventional TED technology.

4. Conclusions

This study demonstrated a non-phase-change approach for the low-temperature drying viscous sludge with high moisture content in a residence time of only a few seconds. By taking advantage of the high-speed self-rotation of the sludge particles in the cyclone dryer and the DPM's dispersion effect on the sludge, the proposed CSRD-based approach noticeably reduced the energy consumed by sludge drying and overcame the disadvantages of conventional TED technology. The impacts of various operating factors on the drying efficiency were deeply examined. The main results obtained from the research work can be summarized as follows:

(1) The smaller the added quartz sand particles, the higher the mixing ratio and the higher the final drying efficiency. However, this is not suitable for the separation process of sludge and quartz sand. The optimal particle size of quartz sand would be in the range of 2–3 mm, and the optimal sand–sludge mixing ratio would be 3:1.

(2) The CSRD process contributed to the fast and efficient drying of viscous sludge at low temperatures. Under the carrier gas temperature of 70 °C, the moisture content of the sludge can be reduced from 80% to below 10%, with a high drying efficiency of more than 95%. The obtained results revealed that the drying efficiency is enhanced by raising the carrier gas temperature and reduced by increasing the feeding rate.

(3) The drying rate of the CSRD-based approach was 522 times higher than that of conventional TED technology. Based on the theoretical calculations, the proportion of non-phase-change of moisture in the CSRD process was 89.26%. This could effectively avoid the latent heat of vaporization that must be overcome in the conventional TED process, thereby reducing the energy consumption for sludge drying.

In summary, the CSRD in a cyclone dryer presents remarkable technical advantages for drying viscous sludge with high moisture content, such as low energy consumption, high efficiency, and time-saving. This groundbreaking research presents an innovative approach to utilizing cyclone separation technology for the effective treatment of sludge. In addition, the innovative approach outlined in the research has the potential to revolutionize how we manage and process sludge, offering more efficient and sustainable solutions for this critical aspect of resource management.

CRediT authorship contribution statement

Junjie Liu: Writing – original draft, Methodology, Data curation. **Qiqi Li:** Writing – original draft, Formal analysis, Data curation. **Yanan Liang:** Visualization, Formal analysis, Data curation. **Jianping Li:** Formal analysis, Data curation. **Yi Liu:** Methodology, Data curation. **Qiong Li:** Methodology, Data curation. **Tingting Cheng:** Writing – review & editing, Validation, Supervision, Resources. **Aosong Wei:** Validation, Supervision, Methodology, Formal analysis. **Shenggui Ma:** Validation, Supervision, Methodology. **Xia Jiang:** Validation, Supervision, Methodology, Conceptualization. **Hualin Wang:** Writing – review & editing, Supervision, Methodology, Conceptualization. **Pengbo Fu:** Writing – review & editing, Supervision, Methodology, Conceptualization.

Declaration of competing interest

The authors declare that they have no known competing financial interests or personal relationships that could have appeared to influence the work reported in this paper.

Acknowledgments

This work was supported by the National Key Research and Development Program of China (2019YFA0705800), the National Natural Science Foundation of China (52030001), and the Science & Technology Commission of Shanghai Municipality (20dz1207600).

Appendix A. Supplementary data

Supplementary data to this article can be found online at https://doi.org/10.1016/j.eng.2024.10.012.

References

[1] Zhou G, Gu Y, Yuan H, Gong Y, Wu Y. Selecting sustainable technologies for disposal of municipal sewage sludge using a multi-criterion decision-making method: a case study from China. Resour Conserv Recycling 2020;161:104881.
[2] Liew CS, Yunus NM, Chidi BS, Lam MK, Goh PS, Mohamad M, et al. A review on recent disposal of hazardous sewage sludge via anaerobic digestion and novel composting. J Hazard Mater 2022;423:126995.
[3] Liu H, Wang X, Qin S, Lai W, Yang X, Xu S, et al. Comprehensive role of thermal combined ultrasonic pre-treatment in sewage sludge disposal. Sci Total Environ 2021;789:147862.
[4] Peccia J, Westerhoff P. We should expect more out of our sewage sludge. Environ Sci Technol 2015;49(14):8271–6.
[5] Zhuang Z, Mohamed BA, Li LY, Swei O. An economic and global warming impact assessment of common sewage sludge treatment processes in North America. J Clean Prod 2022;370:133539.
[6] Wu B, Dai X, Chai X. Critical review on dewatering of sewage sludge: influential mechanism, conditioning technologies and implications to sludge re-utilizations. Water Res 2020;180:115912.
[7] Liu H, Qiao H, Liu S, Wei G, Zhao H, Li K, et al. Energy, environment and economy assessment of sewage sludge incineration technologies in China. Energy 2023;264:126294.
[8] Teoh SK, Li LY. Feasibility of alternative sewage sludge treatment methods from a lifecycle assessment (LCA) perspective. J Clean Prod 2020;247:119495.
[9] Gao D, Wen Z. Phthalate esters in the environment: a critical review of their occurrence, biodegradation, and removal during wastewater treatment processes. Sci Total Environ 2016;541:986–1001.

[10] Cai Q, Mo C, Wu Q, Zeng Q, Katsoyiannis A. Occurrence of organic contaminants in sewage sludges from eleven wastewater treatment plants, China. Chemosphere 2007;68(9):1751–62.
[11] Alvarenga P, Palma P, Mourinha C, Farto M, Dôres J, Patanita M, et al. Recycling organic wastes to agricultural land as a way to improve its quality: a field study to evaluate benefits and risks. Waste Manag 2017;61:582–92.
[12] Aparicio I, Santos JL, Alonso E. Limitation of the concentration of organic pollutants in sewage sludge for agricultural purposes: a case study in South Spain. Waste Manag 2009;29(5):1747–53.
[13] Wei Y, Van Houten RT, Borger AR, Eikelboom DH, Fan Y. Minimization of excess sludge production for biological wastewater treatment. Water Res 2003;37(18):4453–67.
[14] Zhou H, Wei L, Wang D, Zhang W. Environmental impacts and optimizing strategies of municipal sludge treatment and disposal routes in China based on life cycle analysis. Environ Int 2022;166:107378.
[15] Chen H, Jiang H, Zhang W, Peng M, Liu Y, Hu L, et al. The introduction of wet dyeing sludge pellets in the production of clay brick: a novel approach to promote the disposal efficiency. J Clean Prod 2023;385:135675.
[16] Yang G, Zhang G, Wang H. Current state of sludge production, management, treatment and disposal in China. Water Res 2015;78:60–73.
[17] Faragò M, Damgaard A, Logar I, Rygaard M. Life cycle assessment and cost-benefit analysis of technologies in water resource recovery facilities: the case of sludge pyrolysis. Environ Sci Technol 2022;56(24):17988–97.
[18] Bianchini A, Bonfiglioli L, Pellegrini M, Saccani C. Sewage sludge drying process integration with a waste-to-energy power plant. Waste Manag 2015;42:159–65.
[19] Hartman M, Svoboda K, Pohořelý M, Trnka O. Combustion of dried sewage sludge in a fluidized-bed reactor. Ind Eng Chem Res 2005;44(10):3432–41.
[20] Mahmoud A, Olivier J, Vaxelaire J, Hoadley AFA. Electrical field: a historical review of its application and contributions in wastewater sludge dewatering. Water Res 2010;44(8):2381–407.
[21] Zhang X, Ye P, Wu Y. Enhanced technology for sewage sludge advanced dewatering from an engineering practice perspective: a review. J Environ Manage 2022;321:115938.
[22] Cao B, Zhang W, Wang Q, Huang Y, Meng C, Wang D. Wastewater sludge dewaterability enhancement using hydroxyl aluminum conditioning: role of aluminum speciation. Water Res 2016;105:615–24.
[23] Wang D, Liu X, Zeng G, Zhao J, Liu Y, Wang Q, et al. Understanding the impact of cationic polyacrylamide on anaerobic digestion of waste activated sludge. Water Res 2018;130:281–90.
[24] Cao B, Zhang T, Zhang W, Wang D. Enhanced technology based for sewage sludge deep dewatering: a critical review. Water Res 2021;189:116650.
[25] Ling W, Xing Y, Hong C, Zhang B, Hu J, Zhao C, et al. Methods, mechanisms, models and tail gas emissions of convective drying in sludge: a review. Sci Total Environ 2022;845:157376.
[26] Xue K, Li J, Chen H, Xu G, Liu T. Development of a novel power generation system based on the co-combustion of agriculture biomass and sludge integrated with solar-aided sludge drying. Energy Convers Manage 2022;253:115185.
[27] Bennamoun L, Arlabosse P, Léonard A. Review on fundamental aspect of application of drying process to wastewater sludge. Renew Sustain Energy Rev 2013;28:29–43.
[28] Léonard A, Meneses E, Le Trong E, Salmon T, Marchot P, Toye D, et al. Influence of back mixing on the convective drying of residual sludges in a fixed bed. Water Res 2008;42(10):2671–7.
[29] Chen Z, Hou Y, Liu M, Zhang G, Zhang K, Zhang D, et al. Thermodynamic and economic analyses of sewage sludge resource utilization systems integrating drying, incineration, and power generation processes. Appl Energy 2022;327:120093.
[30] Komatsu Y, Sciazko A, Zakrzewski M, Akiyama T, Hashimoto A, Shikazono N, et al. Towards the improvement of thermal efficiency in lignite-fired power generation: concerning the utilization of polish lignite deposits in state-of-the-art IGCC technology. Int J Energy Res 2016;40(13):1757–72.
[31] Sholl DS, Lively RP. Seven chemical separations to change the world. Nature 2016;532(7600):435–7.
[32] Huang Y, Li J, Zhang Y, Wang H. High-speed particle rotation for coating oil removal by hydrocyclone. Separ Purif Tech 2017;177:263–71.
[33] Wang H, Fu P, Li J, Huang Y, Zhao Y, Jiang L, et al. Separation-and-recovery technology for organic waste liquid with a high concentration of inorganic particles. Engineering 2018;4(3):406–15.
[34] Cheng T, Li Q, Wang H, Fang X, Li L, Jiang L, et al. High-speed particle self-rotation in different pre-self-rotation cyclones and application in enhancement of oil recovery from spent catalysts. Separ Purif Tech 2022;296:121430.
[35] Shi D, Huang Y, Wang H, Yuan W, Fu P. Deoiling of oil-coated catalyst using high-speed suspending self-rotation in cyclone. Separ Purif Tech 2019;210:117–24.
[36] Fu P, Wang H, Li J, Huang Y, Fang Y, Yuan W, et al. Cyclonic gas stripping deoiling and gas flow acceleration classification for the resource utilization of spent catalysts in residue hydrotreating process. J Clean Prod 2018;190:689–702.
[37] Li J, Yang X, Ma L, Yang Q, Zhang Y, Bai Z, et al. The enhancement on the waste management of spent hydrotreating catalysts for residue oil by a hydrothermal–hydrocyclone process. Catal Today 2016;271:163–71.
[38] Xu Y, Fang Y, Wang Z, Guo D, Liu Y, Huang Y, et al. *In-situ* sludge reduction and carbon reuse in an anoxic/oxic process coupled with hydrocyclone breakage. Water Res 2018;141:135–44.
[39] Li J, Wang Y, Chang Y, Huang Y, Jiang X, Wang H, et al. Cold model testing of *in-situ* catalyst activation by swirling self-rotation in ebullated bed reactor for biomass pyrolysis oils hydrogenation. Chem Eng J 2021;406:126909.
[40] Ma L, He M, Fu P, Jiang X, Lv W, Huang Y, et al. Adsorption of volatile organic compounds on modified spherical activated carbon in a new cyclonic fluidized bed. Separ Purif Tech 2020;235:116146.
[41] Li Q, Cheng T, Lu Y, Zhang B, Huang Y, Yang Y, et al. Sludge low-temperature drying with mainly non-phase change in mere seconds based on particle high-speed self-rotation in cyclone. Water Res 2022;224:119092.
[42] Fu P, Yu H, Li Q, Cheng T, Zhang F, Yang T, et al. Cyclone rotational drying of lignite based on particle high-speed self-rotation: lower carrier gas temperature and shorter residence time. Energy 2022;244:123005.
[43] Wei A, Zhang T, Fu P, Li J, Wang H. Non-thermal separation of capillary liquid from macropores of solid particle in seconds by cyclone. Sep Purif Technol 2023;333:125731.
[44] Huang Y, Wang H, Tian J, Li J, Fu P, He F. Theoretical study on centrifugal coupling characteristics of self-rotation and revolution of particles in hydrocyclones. Separ Purif Tech 2020;244:116552.
[45] Liu Z, Sun L, Gu X, Wang X, Dong Q, Zhou Z, et al. Characteristics, mechanisms, and environmental LCA of WMA containing sasobit: an analysis perspective combing viscosity–temperature regression and interface bonding strength. J Clean Prod 2023;391:136255.